# On Surf Zone Fluid Dynamics

GEORGE MELLOR[a]

[a] *Program in Atmospheric and Oceanic Sciences, Princeton University, Princeton, New Jersey*

(Manuscript received 27 December 2019, in final form 13 July 2020)

ABSTRACT: There have been several numerical models developed to represent the phase-averaged flow in the surf zone, which is characterized by $kD$ less than unity, where $k$ is wavenumber and $D$ is the water column depth. The classic scenario is that of surface gravity waves progressing onto a shore that create an offshore undertow current. In fact, in some models, flow velocities are parameterized assuming the existence of an undertow. The present approach uses the full vertically dependent continuity and momentum equations and the vertically dependent wave radiation stress in addition to turbulence equations. The model is applied to data that feature measurements of wave properties and also cross-shore velocities. In this paper, both the data and the model application are unidirectional and the surface stress is nil, representing the simplest surf zone application. Breaking waves are described empirically. Special to the surf zone, it is found that a simple empirical adjustment of the radiation stress enables a favorable comparison with data. Otherwise, the model applies to the open ocean with no further empiricism. A new bottom friction algorithm had been derived and is introduced in this paper. In the context of the turbulence transport model, the algorithm is relatively simple.

KEYWORDS: Ocean dynamics; Turbulence; Coupled models; Ocean models

## 1. Introduction

The surf zone is characterized by small $kD$ (where $k$ is wavenumber and $D$ is the water column depth), wherein the waves ''feel'' the bottom; it presents a challenge for numerical ocean models. Archived visual data feature breaking waves with heights of the order of water column depth (Govender et al. 2002). Analytically, the flow is certainly nonlinear and basic theory is in need of empirical augmentation.

An early analytical model was developed by Phillips (1977) for waves impinging normally onto a beach. Wave dissipation was not included so that mean elevation setdown was created as the waves approach the beach. The vertically integrated radiation stress was confined to the surface. Stokes drift was balanced by a vertically constant return flow (undertow); the vertically integrated volume flow must be nil in steady state. A model by Mellor (2013) included the vertically dependent Stokes drift, currents, and the wave radiation stress of Mellor (2003, 2015). The elevation setdown agreed with the Phillips results, but the currents differed substantially. In contrast and as demonstrated below, the inclusion of wave dissipation produces a dominant elevation setup (Bowen et al. 1968). For example, in the models of O'Connor et al. (1998), Garcez-Faria et al. (2000), Apotsos et al. (2007), Newberger and Allen (2007), and Chen et al. (2018), empiricism related to breaking waves and ''rollers'' are included. The first three models parameterize the shape of the undercurrent whereas the latter two models (see section 7) do solve the differential equations for the undercurrent after parameterizing current interaction terms. Reniers et al. (2004) develop a model for water column stress [in this paper and, for example, Kumar et al. (2011) stress is small compared to wave forcing terms]; parameters in the model are adjusted to minimize calculated and measured velocities. Moghimi et al. (2013) compare forcing of the full equations of motion with the radiation stress formalism and with the vortex force formalism. Overall, comparisons with data do not show much difference. Initially, this was surprising to this author who has detailed reasons (Mellor 2016) in favor of the radiation stress forcing. In the vortex force derivation, (McWilliams and J. M. Restrepo 1999; Uchiyama et al. 2010), the curl (differentiation) of the basic equations of motion is executed wherein irrotational parts such as the wave orbital velocities and subsequently the radiation stresses are excluded. Upon ''uncurling'' (integration), irrotational terms other than the original terms are added. A recent finding in Mellor (2017) is that vortex force terms are embedded in the full three-dimensional equations of motion, but they are of lower order compared to the stress radiation terms. The paper by Kumar et al. (2012) apply the vortex force formalism to a surf zone application; included is an alongshore current. Diagnostics show that the vortex force term is small; the momentum equation is predominately forced by an empirical wave breaking term. In the present paper, the alongshore current and the vortex force terms are nil.

Newberger and Allen (2007) used the Princeton Ocean Model (POM) to obtain vertically dependent velocities. Wave interaction including a form of $S_{xx}$ was concentrated at the surface and projected as a vertically constant body force into the water column. Their calculated velocities compared favorably with data. There were no comparisons with elevation data. Their $S_{xx} = E/2D$, which, according to (10) and Longuet-Higgins and Stewart (1964) applies to deep water. A vortex force term was also added to $S_{xx} = E/2D$, which, however, is an order of magnitude smaller.

Chen et al. (2018) also used a three-dimensional circulation model similar to POM but with an unstructured grid. It was coupled to a third generation (Booij and Holthuijsen 1999) wave model. To lowest order in wave parameters [e.g., $(ak)^{-1}\partial a/\partial x$] their radiation stress formulation conforms to the

*Corresponding author*: George Mellor, glmellor@princeton.edu

DOI: 10.1175/JPO-D-19-0318.1

present usage, but they added vastly complicated, higher-order terms together with adjustable roller terms. They compared their model results to the data of Roelvink and Reniers (1995). The plotting resolution was such that comparisons to Fig. 5 below is difficult.

This paper follows that of Kumar et al. (2011), who adopted the stress radiation equation of Mellor (2003) together with the modification of Mellor (2013) wherein the radiation forcing is concentrated near the surface. Their paper and this paper together address different sets of data but are generally consistent. The surface radiation stress modification is here branded as an empiricism unique to the surf zone and not to be applied to the open ocean. What is further detailed in this paper are reasons why the surface modification is required and an analysis of the elements of the equations of motion that relate to the surface elevation—setup versus setdown—and the subsurface circulation, which is characterized by an undertow. Also included here is a new wave-influenced, bottom friction algorithm.[1]

This numerical study of surf zone dynamics, wherein waves progress onto a beach, is cast in a coordinate system wherein $z$ is the vertical coordinate and the one horizontal coordinate is $x$. The idea is to focus on wave breaking and wave–circulation interaction processes and turbulence exchange applicable to the surf zone while, at the same time, leaving the basic algorithm unaltered when dealing with open ocean dynamics.

In section 2, the equations of motion, reduced to two dimensions, are reviewed. In section 3, the three-dimensional wave radiation stress and its two-dimensional version is also reviewed. Models for bottom dissipation and bottom-induced, breaking wave dissipation are presented. In section 4, solutions of the equations of motion with the unaltered wave radiation stress are presented; the elevation solution was satisfactory but the currents were less than satisfactory compared with the data of Roelvink and Reniers (1995). The strong nonlinearities ascribed to breaking waves in the surf zone suggest the need for an empirical modification of the radiation stress term for small $kD$. Section 5 presents results of the modification, which is constrained such that the vertical integral of the radiation stress and therefore the elevation solution is unchanged. The current distribution, vertically and horizontally, is significantly improved. Application of the modified radiation stress to general ocean problems is discussed in section 6. Section 7 concludes with a summary.

## 2. The governing equations

In this paper, we deal with a simple application wherein the flow is unidirectional and planar and surface stress is nil. Thus, the equation governing the transport and decay of wave energy $E$ is

$$\frac{\partial E}{\partial t} + \frac{\partial}{\partial x}[(c_g + u_A)E] + \int_{-1}^{0} S_{xx}\frac{\partial U}{\partial x} D d\varsigma = -D_{\mathrm{BF}} - D_{\mathrm{WBR}}, \quad (1)$$

where we deal with monochromatic waves of frequency $\sigma = kc$; $k$ is the wavenumber, $c$ is the phase speed, and $c_g = \partial\sigma/\partial k$ is the group speed governed by the dispersion relation

$$\sigma^2 = gk \tanh kD, \quad (2a)$$

$$c_g = c\left(\frac{1}{2} + \frac{kD}{\sinh 2kD}\right). \quad (2b)$$

The water column depth is $D \equiv h + \hat{\eta}$, where $h$ is the still water depth and $\hat{\eta}$ is the mean dynamic elevation. The advective speed is $u_A$, but in this paper is negligibly small. For unidirectional flow $S_{xx}$ is the governing component of the radiation stress tensor. The two terms on the right side of (1) are dissipation due to bottom friction and bottom-induced wave breaking, respectively. The velocity $U$ is defined below. In keeping with the simplicity of the forcing, there is no wind stress or wave energy source and these terms have been removed from (1).

An important parameter is $kD$. For deep water, $kD$ is large so that $\sigma^2 = gk$ and $c_g = c/2 = (g/k)^{1/2}$ whereas, for shallow water, $kD$ is small so that $\sigma^2 = kDgk$ and $c_g = c = (gD)^{1/2}$. The surf zone is characterized by $kD \le 1$.

Governing the behavior of surface elevation and currents are the phase-averaged continuity equation

$$\frac{\partial DU}{\partial x} + \frac{\partial \Omega}{\partial \varsigma} + \frac{\partial \hat{\eta}}{\partial t} = 0, \quad (3)$$

and the momentum equation

$$\frac{\partial DU}{\partial t} + \frac{\partial DU^2}{\partial x} + \frac{\partial \Omega U}{\partial \varsigma} + \frac{\partial DS_{xx}}{\partial x} + gD\frac{\partial \hat{\eta}}{\partial x} = \frac{\partial \tau}{\partial \varsigma}, \quad (4a)$$

$$\tau = \frac{K_M}{D}\frac{\partial \hat{u}}{\partial \varsigma}. \quad (4b)$$

Eqs. (3) and (4) are in "sigma" coordinates whereby $\varsigma = (z - \hat{\eta})/(h + \hat{\eta})$ instead of $\sigma$, which is needed to represent frequency. At the mean surface, $z = \hat{\eta}$ or $\varsigma = 0$; at the bottom, $z = -h$ or $\varsigma = -1$. In this paper's application, the surface stress is nil so that $\tau\ (\varsigma = 0) = 0$. The three-dimensional Stokes drift (Phillips 1977) is

$$(u_{Sx}, u_{Sy}) = \frac{2(k_x, k_y)E}{c}\frac{\cosh 2kD(1+\varsigma)}{\sinh 2kD}, \quad w_{Sz} = 0. \quad (5)$$

In this study, $(k_x, k_y) = (k, 0)$ and $(u_{Sx}, u_{Sy}) = (u_S, 0)$. For unidirectional flow, $U = \hat{u} + u_S$; $\hat{u}$ is the Eulerian mean velocity and $u_S$ is the Stokes drift. Specification of $K_M$ is in appendix A. Reasons why $\hat{u}$ is the dependent variable rather than $U$ in (4b) are in Mellor (2013). The velocity normal to sigma surfaces is $\Omega$ such that the vertical boundary conditions are $\Omega = 0$ at $\varsigma = 0$ and $\varsigma = -1$.

Near the bottom, an enhanced law of the wall, discussed in appendix B, is

$$(\hat{u}, \hat{v}) = \frac{u_\tau}{S_M q}\frac{(\tau_x \tau_y)}{u_\tau}\frac{1}{\kappa}\ln\left(\frac{z'}{z_0}\right), \quad (6a)$$

[1] And which is derived from the turbulence closure model of Mellor and Yamada (1982). Oddly, Kumar et al. (2011) relate internal Reynolds stress to mixing coefficients but supply no further details.

where $z' = h + z$ is measured from the bottom. The friction velocity is $u_\tau = \tau^{1/2} = (\tau_x^2 + \tau_y^2)^{1/4}$; $\kappa = 0.40$ is von Kármán's constant, and $q^2/2$ is the turbulence kinetic energy as detailed in appendix A. The model constant $S_M = 0.39$ (Mellor and Yamada 1982). Wave breaking energy is transferred to turbulence kinetic energy in which case $S_M q/u_\tau$ is variable. In the absence of waves (see appendix B), $S_M q/u_\tau = 1.0$. Derived from (6a), the form that is used in the model is

$$(\tau_x, \tau_y) = K_M\left(\frac{\partial \hat{u}}{\partial z}, \frac{\partial \hat{v}}{\partial z}\right) = \left(\frac{S_M q}{u_\tau}\right)^2 \left(\frac{\kappa}{\ln z'/z_0}\right)^2 |\hat{\mathbf{u}}|(\hat{u}, \hat{v}), \tag{6b}$$

where $|\hat{\mathbf{u}}| = (\hat{u}^2 + \hat{v}^2)^{1/2}$. In this paper, $(\hat{u}, \hat{v}) = (\hat{u}, 0)$ and $(\tau_x, \tau_y) = (\tau, 0)$. All variables apply to the nearest bottom grid points. The second and third equality in (6b) is used in the model as the bottom boundary conditions for (4).

## 3. The standard radiation stress and dissipation

In this paper, discussion and analyses are focused on the radiation stress term $S_{xx}$ and parameterizations of the wave dissipation terms $D_{\mathrm{BF}}$ and $D_{\mathrm{WBR}}$. An important part of the paper is the turbulent energy equations that determine the turbulence transfer coefficient $K_M$. It is separately dealt with in appendix A.

### a. The standard wave radiation stress

Since the waves in the ensuing experiment are quite narrow banded and to simplify discussion, it is deemed appropriate to base the vertically dependent wave radiation stress on monochromatic waves. Thus, the radiation stress expression obtained by Mellor (2003, 2015) is

$$S_{\alpha\beta} = kE\left(\frac{k_\alpha k_\beta}{k^2} F_{CC} F_{CS} - \delta_{\alpha\beta} F_{SS} F_{SC}\right) + \delta_{\alpha\beta} \Im(\varsigma), \tag{7a}$$

$$\Im(\varsigma) = \frac{E}{2D}\frac{\partial}{\partial \varsigma}(2F_{CC}F_{SS} - F_{SS}^2), \tag{7b}$$

where, also

$$\Im(\varsigma) = kE(F_{SC}F_{SS} + F_{CC}F_{CS} - F_{SS}F_{CS}). \tag{7c}$$

In (7a) and (7b), $\alpha$ or $\beta = x$ or $y$. Convenient definitions are

$$F_{CC} = \frac{\cosh kD(1+\varsigma)}{\cosh kD}, \tag{8a}$$

$$F_{CS} = \frac{\cosh kD(1+\varsigma)}{\sinh kD}, \tag{8b}$$

$$F_{SS} = \frac{\sinh kD(1+\varsigma)}{\sinh kD}, \tag{8c}$$

$$F_{SC} = \frac{\sinh kD(1+\varsigma)}{\cosh kD}. \tag{8d}$$

Note that, from (7b) or (7c), $\int_{-1}^{0} \Im d\varsigma = E/2D$. Although a detail in the Mellor (2003) derivation is corrected in Mellor (2015), the results are the same. Thus, combining (7a) and (7c), we obtain $S_{\alpha\beta} = kE[(k_\alpha k_\beta/k^2)F_{CC}F_{CS} + \delta_{\alpha\beta}(F_{CS}F_{CC} - F_{SS}F_{CS})]$ as in the 2003 paper. Prior to Mellor (2003), the depth-dependent relations in (7a) and (7b) were not available.

In this paper, the problem is simplified to unidirectional flow so that (7) is

$$S_{xx} = \frac{2kE}{\sinh 2kD} + \Im(\varsigma), \tag{9}$$

and $\Im(\varsigma)$ is not altered from that in (7b) or (7c). The vertically dependent asymptotic behavior of $S_{xx}$ is as $kD \to 0$, $S_{xx} = E/D + \Im$; $\Im = -(E/D)\varsigma$, and as $kD \to \infty$, $S_{xx} = 0 + \Im$; $\Im = kE\exp(2kD\varsigma)$. The vertical integral of (9) is

$$\int_{-1}^{0} S_{xx} d\varsigma = \frac{E}{D}\left(\frac{1}{2} + \frac{2kD}{\sinh 2kD}\right) = \frac{E}{D}\left(2\frac{c_g}{c} - \frac{1}{2}\right) \tag{10}$$

in agreement with Longuet-Higgins and Stewart (1964) and Phillips (1977).

### b. Bottom dissipation

In (1), the term $D_{\mathrm{BF}}$ is the wave energy dissipation due to bottom friction, which is enhanced by oscillatory wave motion. In Booij and Holthuijsen (1999), one has

$$D_{\mathrm{BF}} = C_b u_b^3 = C_b \frac{\sigma^3 (2E/g)^{3/2}}{\sinh^3 kD}, \tag{11}$$

where $u_b = a\sigma/\sinh kD$ is the wave velocity amplitude near the bottom. The form of (11) has also been derived by Mellor (2002) where, additionally, the factor, $C_b$ is given by

$$C_b \times 10^4 = 0.7xl^2 + 4.0xl + 6.5, \tag{12}$$

where $xl = \log_{10}(\sigma z_0/u_b)$. For example, for $\sigma z_0/u_b = 10^{-3}$ or $10^{-4}$, and $C_b = 0.8 \times 10^{-4}$ or $1.7 \times 10^{-4}$.

### c. Breaking wave dissipation

For a wave progressing into shallow water, Battjes and Janssen [1978; also see an appendix in Booij and Holthuijsen (1999) for a detailed discussion] provide

$$D_{\mathrm{WBR}} = \frac{g\sigma}{8\pi} Q_b H_M^2, \tag{13}$$

where the wave breaking probability function $Q_b$ is given by the transcendental relation,

$$(Q_b - 1)/\ln Q_b = 8(E/g)/H_M^2, \tag{14a}$$

$$H_M \equiv \gamma D. \tag{14b}$$

As empirically determined by Booij and Holthuijsen (1999), $\gamma = 0.7$ and in agreement with data–model comparisons in Mellor et al. (2008) and Marsooli et al. (2017). In the numerical code, (14) is solved iteratively, but to understand its behavior, Table 1 is offered. Defining a significant wave height, $H_S = 4(E/g)^{1/2}$, the right side of (14a) may be simply written $H_S^2/D^2$ since $\gamma^2 = 0.5$. In the following numerical simulations, the largest value of $H_S^2/D^2 = 0.584$.

## 4. Wave and current development; first trial

The three-dimensional Princeton Ocean Model (Blumberg and Mellor 1987) is used to integrate (1), (3), (4), and (7); its

TABLE 1. Solutions of (14), solved iteratively using $Q = \exp[(Q-1)/(8E/gH_M^2)]$.

| $8(E/g)/H_M^2$ | 0.1 | 0.2 | 0.3 | 0.4 | 0.5 | 0.6 | 0.7 | 0.8 | 0.9 | 1.0 |
|---|---|---|---|---|---|---|---|---|---|---|
| $Q_b$ | 0.000 | 0.001 | 0.041 | 0.107 | 0.203 | 0.324 | 0.463 | 0.629 | 0.805 | 1.000 |

computational spatial indices are $i$, $j$, $k$, but is here rendered two-dimensional with indices $i$, $k$. Calculations are compared to data obtained by Roelvink and Reniers (1995) in a large wave tank, the "Delta Flume," to evaluate coupled circulation–wave models. The laboratory wave tank was 233 m long, 5 m wide, and 7 m deep. The bottom whose profile is shown in Fig. 1 was made of concrete overlaid with sand with a median grain diameter of 0.22 mm so that the bottom roughness length $z_0$ is set to $2 \times 10^{-5}$ m. Experimental runs were conducted under different incident wave conditions, including slightly erosive, highly erosive, and strongly accretive wave conditions. Waves were created by a piston-type wavemaker. We compare the model results with measurements from the slightly erosive experiment 1A, forced by the narrow-band waves with an upstream, significant wave height of 0.96 m, a wave period of 5 s, and a still water depth of 4.1 m.

The vertical computational grid consists of 20 vertical layers; the increments of the top layers from 5 to 1 are reduced logarithmically upward. The horizontal grid spacing is 5 m reduced to 2.5 m as the shallow end is approached. Calculations with double the horizontal spacing were unchanged within plotting resolution. The split time step for waves is 0.10 s; for the external mode step, 0.05 s and for the internal mode step, 0.20 s. The measured water surface elevation and wave properties offshore are used as the model boundary conditions. A radiation velocity condition is applied to the offshore boundary; inshore, the velocity is zero. The simulation model time to steady state was 25 min and the model was run for 50 min.

The balance of terms for Eq. (1) is simple; the third term on the left is negligible as is $u_A$ relative to $c_g$ and dissipation due to bottom friction is quite small; thus, $\partial(c_g E)/\partial x \cong -D_{\mathrm{WBR}}$ after steady state is obtained.

Figure 1 shows the bottom topography, the development of the significant wave height where $H_S = 4(E/g)^{1/2}$ and the elevation height. Comparison of the wave height and elevation with data are deemed to be satisfactory.

Figure 2a is a diagnostic plot of vertically integrated, wave radiation stress gradient, which is nearly balanced by the elevation gradient since the bottom stress and the gradient of momentum are quite small. In the range, $0 < x < 60$ m, the elevation gradient is negative, evidence of setdown. However, the computed setdown in Fig. 1c is small and not seen in the tank data. Beyond $x = 60$ m, breaking dissipation dominates and setup develops. In a model run (not shown) with no wave breaking dissipation, setdown prevails.

The resulting onshore/offshore flow is compared with measurements in Fig. 3. The comparison is with the Eulerian mean velocity appropriate to measurements since, at a fixed point, $T^{-1}\int_0^T(\hat{u} + kacF_{CS}\cos\sigma t)\,dt = \hat{u}$ for large $T$; thus, $u_S$ is subtracted from $U$.

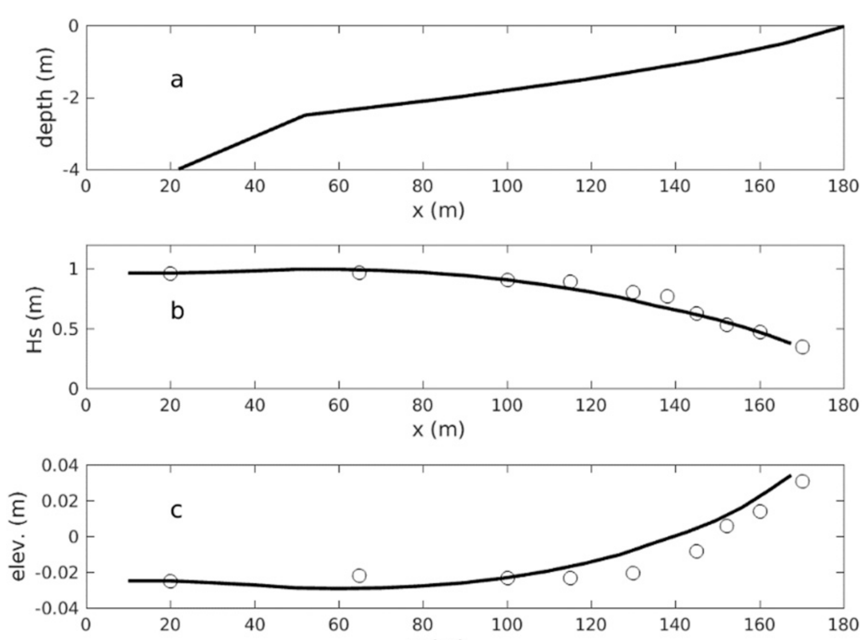


FIG. 1. Calculations (solid lines) from (1), (3), (4), and (7) and data (circles) from Roelvink and Reniers (1995): (a) the bottom topography, (b) significant wave height, and (c) mean elevation height.

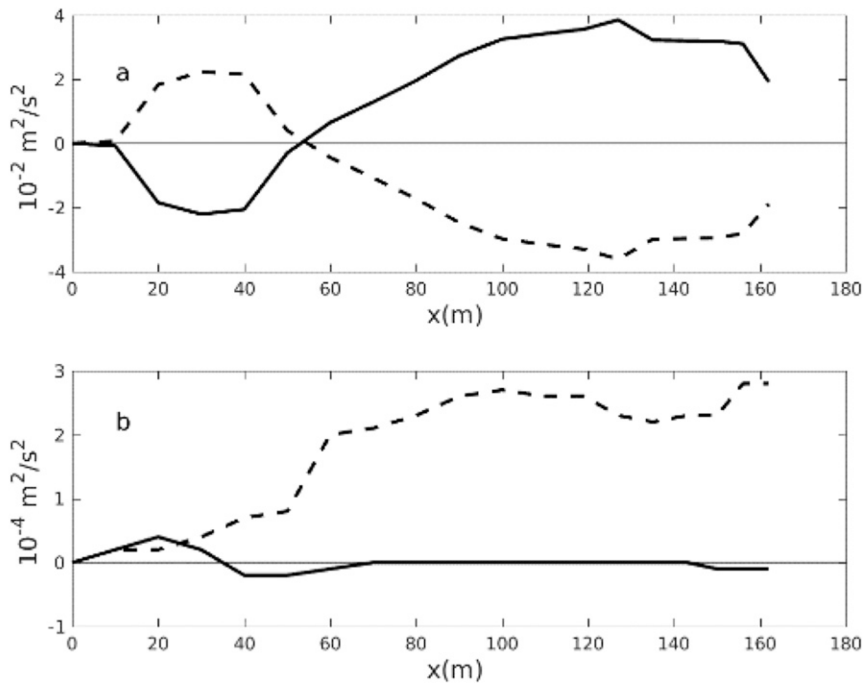


FIG. 2. The terms in Eq. (4) integrated from $\varsigma = -1$ to $\varsigma = 0$: (a) $\int_{-1}^{0}(gD\partial\hat{\eta}/\partial x)\,d\varsigma = gD\partial\hat{\eta}/\partial x$ (solid line) and $\partial(\int_{-1}^{0} DS_{xx}d\varsigma)/\partial x$ (dashed line); (b) $\int_{-1}^{0}(\partial\tau/\partial\varsigma)\,d\varsigma =$ bottom stress (dashed line) and $\partial(\int_{-1}^{0} DU^2 d\varsigma)/\partial x$ (solid line). The variables in (b) are order $10^{-2}$ smaller than those in (a). The sum of all four terms is nil.

Although there is undertow in Fig. 3, clearly the correspondence between calculations and data in Fig. 3 is not satisfactory. The problem is evident in Fig. 4. For large $kD$, the forcing by $S_{xx}$ is greater near the surface; in fact $S_{xx}$ is proportional to $e^{2kD\varsigma} = e^{2k(\hat{\eta}-z)}$ for $kD > 3$. But, for $kD < 1$ as is the case in the surf zone, the opposite is true; e.g., for $kD < 0.25$, $S_{xx}$ is proportional to $1 - \varsigma/2$ so that the forcing by $S_{xx}$ is greater near the bottom.

## 5. Empirically modified wave radiation stress; second trial

When waves are breaking as strongly as they do in the surf zone, it might be expected that $S_{xx}$ or $u_S$, as derived from linear theory, would not be adequate to simulate the flow. Some kind of empirical modification is required.[2] Concentrating momentum near the surface via a "roller" model were elements of the models by Garcez-Faria et al. (2000), Newberger and Allen 2007, and Reniers et al. (2004) and others. The introduction of rollers and other surface-concentrated, wave–current interaction terms suggested a trial whereby $\Im(\varsigma)$ in (9) is replaced by $(E/2D)\delta_{\mathrm{DIR}}(0)$ so that

$$S_{xx} = \frac{2kE}{\sinh 2kD} + \frac{E}{2D}\delta_{\mathrm{DIR}}(0), \tag{15}$$

where $\delta_{\mathrm{DIR}}$ is a Dirac delta function such that $\int_{-1}^{0}\delta_{\mathrm{Dir}}d\varsigma = 1$, but $\delta_{\mathrm{Dir}}(\varsigma) = 0,\ \ \varsigma \neq 0$. In a finite difference approximation, one would interpret $\delta_{\mathrm{DIR}}(k) = 1/d\varsigma\,(k)$ for $k = 1$, otherwise $\delta_{\mathrm{DIR}}(k) = 0$ for $k > 1$.[3] Thus, some $S_{xx}$ forcing is concentrated at the surface; nevertheless, the integrated value of $S_{xx}$ is preserved, which proved adequate in simulating elevation for the present case but also other surf zone cases in Marsooli et al. (2017). Somewhat ironically, the $\delta_{\mathrm{DIR}}$ term was once (Mellor 2011) considered correct, but subsequently was found incorrect due to an error in evaluating pressure within the trough-to-crest wave region [an error also found in Longuet-Higgins and Stewart (1964), which, however, did not alter their vertically integrated result as is the case here].

Use of the delta function might be considered somewhat severe, but as seen in Fig. 5, the calculated results compare reasonable well with the data and is a significant improvement relative to Fig. 3. The empirical modification in (15) is similar to that in Kumar et al. (2011).

## 6. Empirically modified wave radiation stress

Aside from the fact that the strategy of replacing $\Im(\varsigma)$ with a surface delta function does improve profiles, one wishes to preserve the unchanged $S_{xx}$ for large $kD$ deemed appropriate for the open ocean. Thus,

[2] A hint is provided by the paper by Marsooli et al. (2017), who used a variation of (8b), which resulted in calculations more realistic than obtained in Fig. 3.

[3] Or if $\delta_{\mathrm{DIR}}(k) = 0.5/d\zeta(k)$ for $k = 1$ and 2 there was negligible differences in the calculated result. Other surface distributions splits were not investigated.

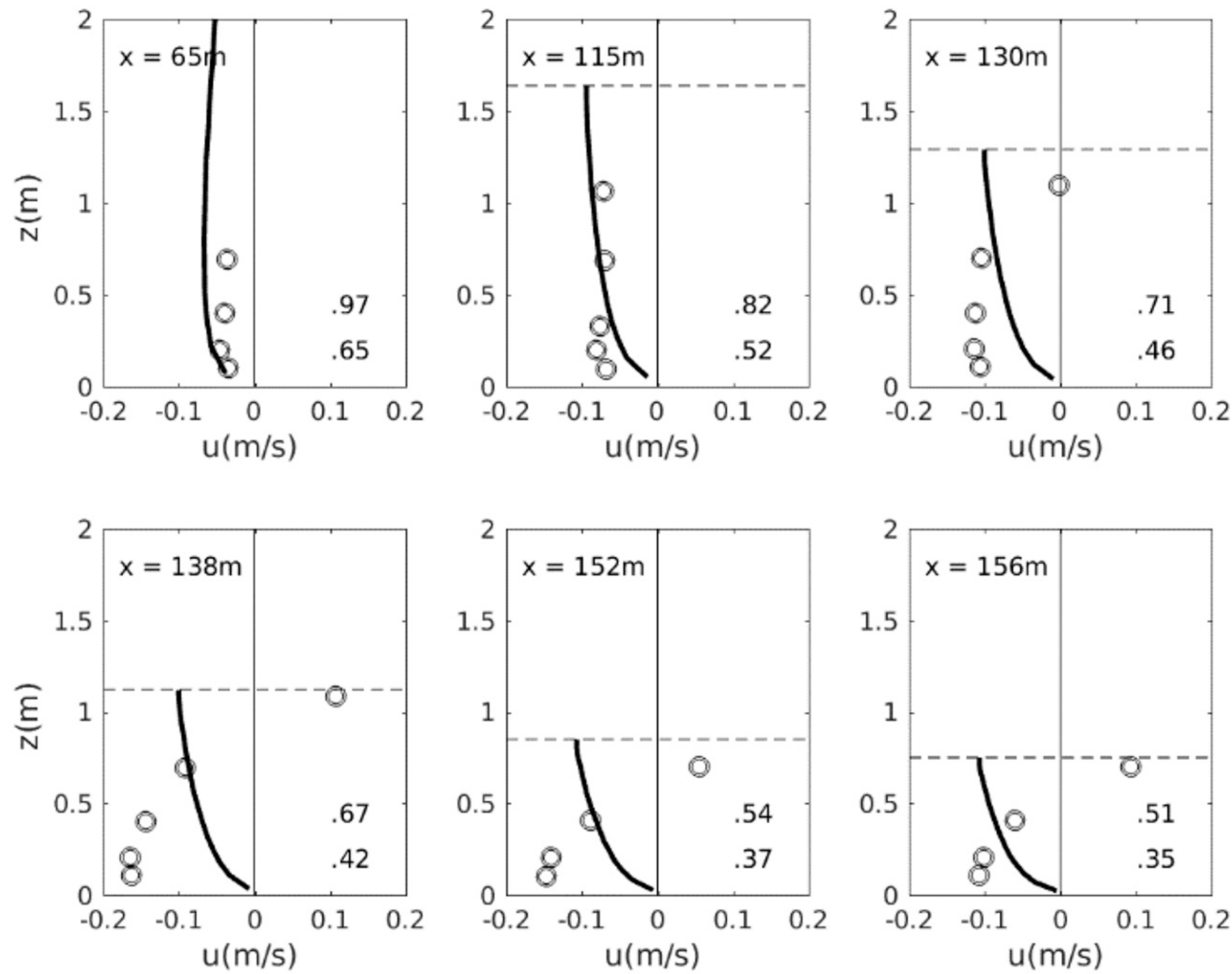


FIG. 3. The velocity profiles of $\hat{u} = U - u_S$ showing a clear mismatch of data (circles) and calculations (lines). Here $z$ is measured from the bottom. The horizontal dashed lines denote the mean surfaces, except for $x = 65$ m where the mean surface = 2.29 m. The calculations are from (3) and (4) using $S_{xx}$ from (7) and (8b). The values of (top) $H_S$ and(bottom) $kD$ are shown in the lower-right corner for each profile. The calculations here correspond to $\Gamma = 0$ in Eq. (16).

$$S_{xx} = kE(F_{CC}F_{CS} - F_{SS}F_{SC}) + (1-\Gamma)\Im(\varsigma) + \Gamma\frac{E}{2D}\delta_{\mathrm{DIR}}(0). \tag{16}$$

Evidently $\Gamma = 0$ shoreward of the surf zone where $kD$ is large, but $\Gamma > 0$ inside the surf zone where $kD$ is small. Importantly, the integral, $\int_{-1}^{0} DS_{xx}d\varsigma$ is preserved for all $\Gamma$ as are the integrated results of Fig. 1. With (16) defined, the calculations in Fig. 3 correspond to $\Gamma = 0$ whereas in Fig. 5, $\Gamma = 1$.

How does $\Gamma$ vary from the value 0 to the value 1 and should its dependency be on $kD$, $H_S/D$ (or derivable quantities), or $Q_b$? Consider $\Gamma = \Gamma(H_S/D)$. From Table 2, one presumes that $\Gamma \cong 0$for $H_S/D$ for, say, less than 0.4 and $\Gamma \cong 1$ for, say, $H_S/D$ greater than 0.5. Therefore, a very simple scheme is

$$\Gamma = \begin{pmatrix} 0, & H_S/D \le 0.4 \\ 1, & H_S/D > 0.4 \end{pmatrix}. \tag{17}$$

Equation (17) satisfies the criteria stated above. It is a placeholder until more analyses and/or relevant data become available. Possibly, $\Gamma$ might be a function of other variables such as bottom slope. Small variations of (17) do not change the results in Fig. 5.

A test case (not shown) has been run wherein $12 > kD > 1$ and $\Gamma = 0$ and no wave breaking. A robust undertow is obtained.

## 7. Summary

The paper by Phillips (1977, section 3.7) describes a unidirectional model whereby the wave driven Stokes drift is confined to the surface; the return flow, the undertow, is vertically constant and is prescribed to satisfy zero vertically integrated onshore velocity. An extension by Mellor (2013) includes a vertically dependent radiation stress and currents; nevertheless, the mean elevation agreed with the Phillips result, but currents differed substantially. Wave

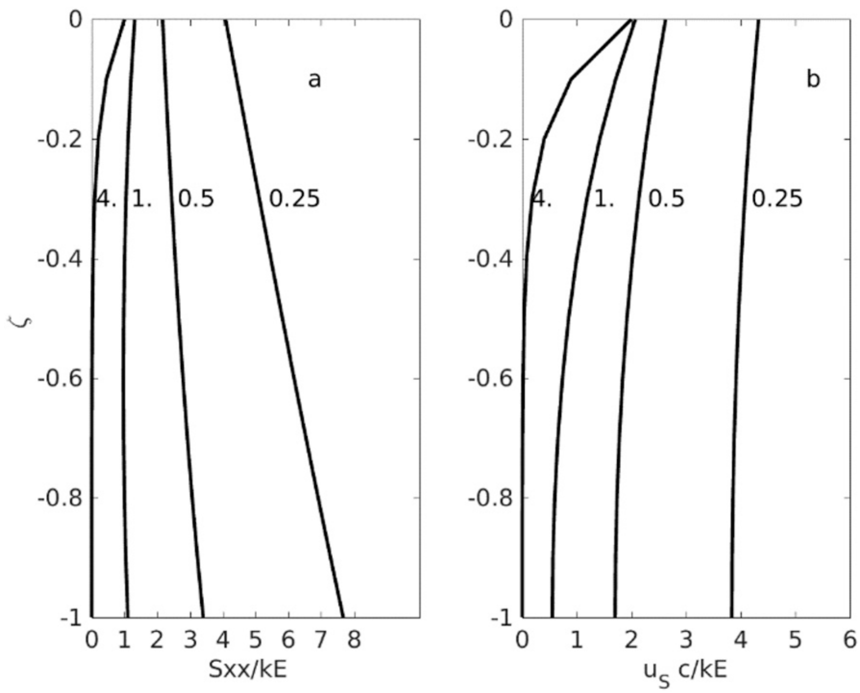


FIG. 4. (a) Sample profiles of $S_{xx}$ normalized by $kE$. The value of $kD$ is shown for each profile. (b) The Stokes drift profiles normalized by $kE/c$.

breaking dissipation was excluded in both papers and mean elevation setdown was the result. In the present paper wave breaking is included and wave elevation is dominated by wave setup (Bowen et al. 1968).

In summary:

1) Wave energy advection is balanced by wave breaking dissipation here described by the findings of Battjes and Janssen (1978).
2) A property of the radiation stress is that the gradient of the vertically integrated radiation stress—equal to that by Longuet-Higgins and Stewart (1964) and Phillips (1977)—balances the mean elevation gradient; i.e., $\partial D(\int_{-1}^{0} S_{xx} d\varsigma)/\partial x = -gD\partial\hat{\eta}/\partial x$.
3) To simulate vertical current structure, the vertical structure of the wave radiation stress (Mellor 2003, 2015) required empirical modification since the momentum equation (4) essentially reduces to

$$\frac{\partial}{\partial x} D\left(S_{xx} - \int_{-1}^{0} S_{xx} d\varsigma\right) = \frac{\partial}{\partial\varsigma}\left(\frac{K_M}{D}\frac{\partial\hat{u}}{\partial\varsigma}\right). \qquad (18)$$

The modification is meant to account for the strong nonlinearities associated with the breaking waves. Sample profiles of $K_M$ are in Fig. 6. It is noted that $K_M$ for the flows for $\Gamma = 0$ in Fig. 3 do not differ from the flows for $\Gamma = 1$ in Fig. 5 so that differences in the two solutions are almost entirely due to the deviation of $S_{xx}$ from its vertical mean as in (18). Fortunately, excellent data by Roelvink and Reniers (1995) are available to provide flow velocities featuring undertow.

This entire paper has been applied to unidirectional flow. In the more general, three-dimensional ocean applications, the wave radiation stress is

$$S_{\alpha\beta} = kE\left(\frac{k_\alpha k_\beta}{k^2} F_{CC}F_{CS} - \delta_{\alpha\beta}F_{SS}F_{SC}\right) + \delta_{\alpha\beta}\left[(1-\Gamma)\Im(\varsigma) + \Gamma\frac{E}{2D}\delta_{\mathrm{DIR}}(0)\right] \qquad (19)$$

and where $\Gamma = 0$ offshore and $\Gamma = 1$ inshore as in, for example, Eq. (17).

*Acknowledgments.* Comments by two reviewers contributed to an improved paper.

## APPENDIX A

### The Turbulence Equations

The model as discussed above requires knowledge of the turbulence momentum mixing coefficient given by $K_M = S_M q\ell$ (Mellor and Yamada 1982, hereafter MY82), where $q$ is obtained from

$$\frac{\partial Dq^2}{\partial t} + \frac{\partial DUq^2}{\partial x} + \frac{\partial DVq^2}{\partial y} + \frac{\partial \Omega q^2}{\partial\varsigma} = \frac{\partial}{\partial\varsigma}\left(\frac{K_q}{D}\frac{\partial q^2}{\partial\varsigma}\right) + 2D(P_S + P_B + \varepsilon) + 2D_{\mathrm{WBR}}f, \qquad (\mathrm{A1})$$

where $q^2/2$ is the turbulence kinetic energy. Another equation in MY82 provides the turbulence length scale $\ell$ (not shown). In

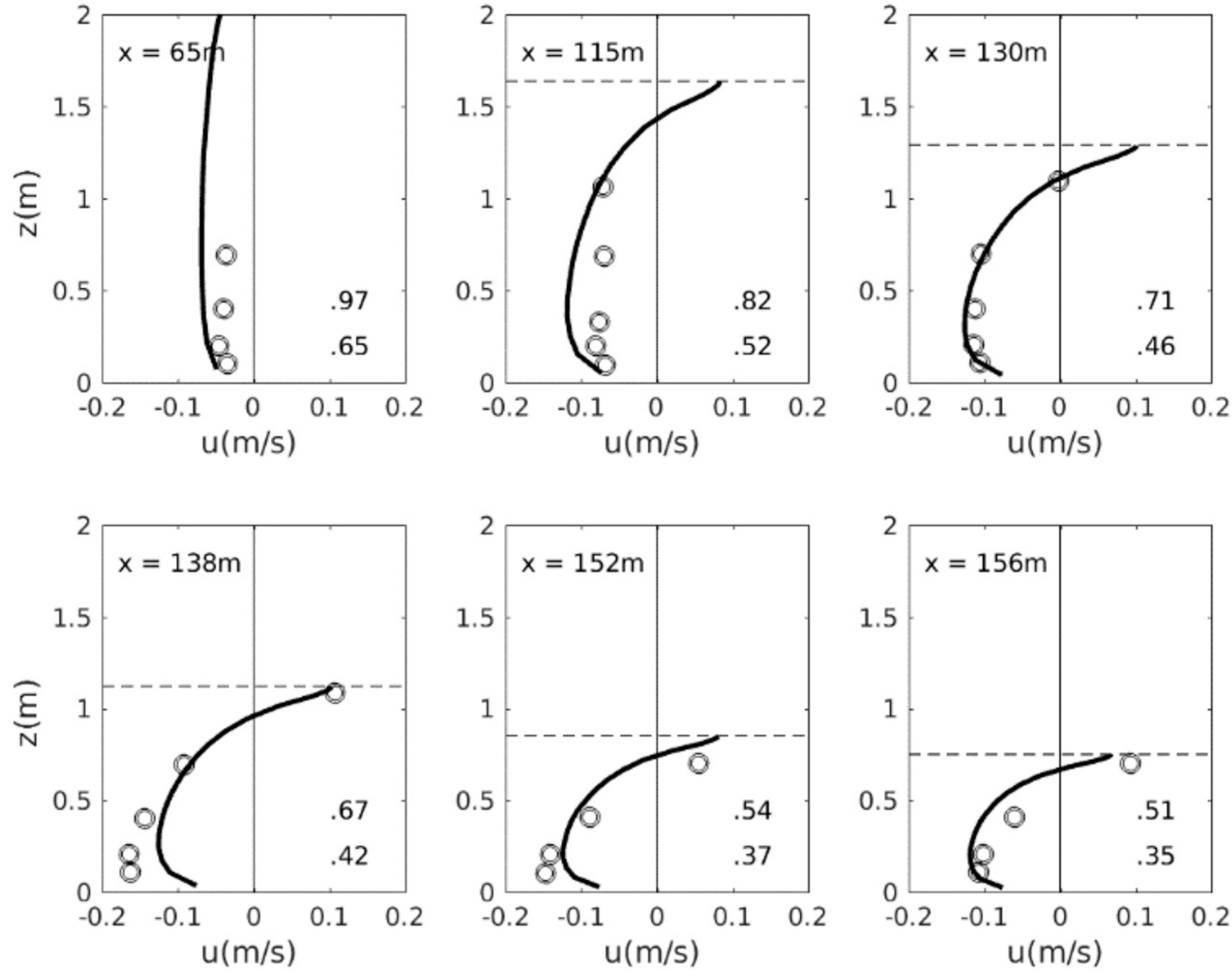


FIG. 5. Profiles of $\hat{u} = U - u_S$ for the data (circles) and calculations (lines). Here $z$ is measured from the bottom. The horizontal dashed lines denote the mean surfaces, except for $x$ = 65 m where the mean surface = 2.29 m. Calculations here are from (3) and (4) using $S_{xx}$ from (15). The values of (top) $H_S$ and (bottom) $kD$ are shown in the lower-right corner for each profile The calculations here correspond to $\Gamma = 1$ in Eq. (16).

that equation, $\ell = H_S$ has been used as the surface boundary condition. Sample plots of $q^2$, $\ell$, and $K_M$ for $x$ = 130 m are in Fig. 6.

The expressions for the shear production $P_S$ and buoyancy production $P_B$ (=0 in this application) are in MY82. The term $D_{\mathrm{WBR}}f$ from (13) has been added to (A1). It is added to (A1) under the assumption that some (or all) of the breaking wave dissipation is manifest as large-scale turbulence in the water column. Some improvement in the profiles of Fig. 5 have been obtained if approximately half of $D_{\mathrm{WBR}}$ is applied to (A1) so that $\int_{-1}^{0} f d\varsigma = 1/2$. Whether distributed uniformly so that $f$ = 1/2 or biased toward the surface so that $f = (1 - \varsigma)$ made negligible difference in the results; the latter has been implemented in all calculations.

The small dissipation $D_{\mathrm{BF}}$ due to bottom friction, discussed below, has been added to (A1) as a diffusion, bottom boundary condition.

## APPENDIX B

### The Bottom Friction

The influence of waves on bottom friction has generally been taken into account by modifying the roughness $z_0$ (Grant and Madsen 1979). In the present framework wherein turbulence properties are available, an alternate algorithm (Mellor 2002) is available. It consists of Eqs. (11) and (12),

TABLE 2. Parameters related to breaking waves. The initial values at $x$ = 10 m plus those corresponding to the locations of profile in Figs. 3 and 5.

| $x$ (m) | 10 | 65 | 115 | 130 | 138 | 152 | 158 |
|---|---|---|---|---|---|---|---|
| $kD$ | 0.90 | 0.65 | 0.52 | 0.47 | 0.43 | 0.37 | 0.35 |
| $H_s/D$ | 0.22 | 0.43 | 0.54 | ,57 | 0.59 | 0.65 | 0.67 |
| $Q_b$ | 0.000 | 0.005 | 0.036 | 0.059 | 0.074 | 0.135 | 0.163 |

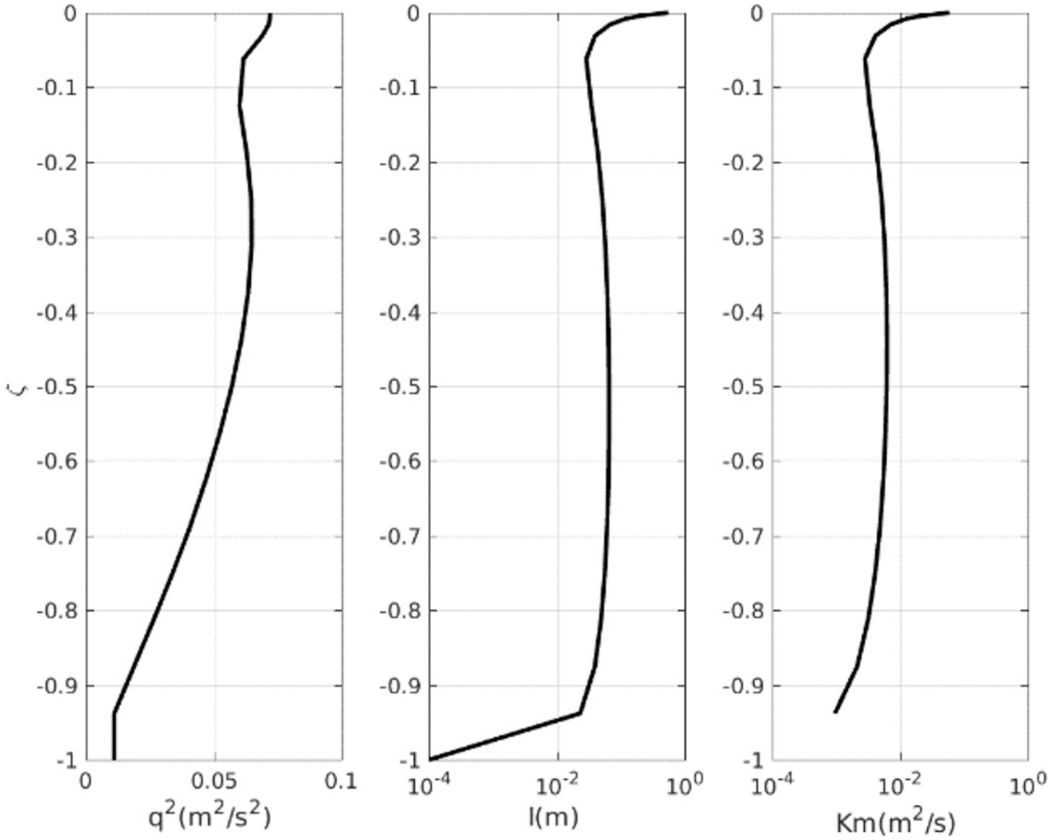


FIG. 6. The profiles of $q^2$, $\ell$, and $K_M$ as functions of $\zeta$ at $x = 130$ m. The boundary condition for $\ell(\varsigma)$ is $\ell = H_S$ at $\varsigma = 0$ and is responsible for the behavior of $\ell$ and $K_M$ near $\zeta = 0$. The results are for $\Gamma = 1$, but do not differ significantly from the results for $\Gamma = 0$.

where, in this paper, a simplification is that the bottom friction dissipation $D_{BF}$ has been included as a bottom diffusion term. Also, a generalization of the law-of-the-wall is introduced in (6a) and (6b). Thus, from MY82, $K_M = S_M q \ell$ so that

$$(\tau_x, \tau_y) = S_M q \ell \left(\frac{\partial \hat{u}}{\partial z}, \frac{\partial \hat{v}}{\partial z}\right). \quad \text{(B1)}$$

Equation (B1) applies throughout the water column. However, near a solid surface and by definition, $\tau \equiv u_\tau^2$ and $\ell \equiv \kappa z$. An integral of (B1) is

$$(\hat{u}, \hat{v}) = \frac{u_\tau}{S_M q} \frac{(\tau_x, \tau_y)}{u_\tau} \frac{1}{\kappa} \ln\left(\frac{z'}{z_0}\right), \quad \text{(B2)}$$

where the constant of integration is $z_0$ and is the conventional surface roughness. The factor $S_M q/u_\tau$ is the aforementioned generalization. In the absence of waves, $S_M q/u_\tau = 1$[B1] and the result is that (B2) reduces to the more conventional law-of-the-wall. But, in the presence of waves, $S_M u_\tau/q$ is generally less than unity due to the additional wave breaking term $D_{WBR}$ in (A1).

From (B2), one can form, $|\hat{\mathbf{u}}| = (\hat{u}^2 + \hat{v}^2)^{1/2} = u_\tau(u_\tau/S_M q) \ln(z'/z_0)/\kappa$. Eliminating, $u_\tau$ in favor of $|\hat{\mathbf{u}}|$ yields

$$(\tau_x, \tau_y) = K_M \left(\frac{\partial \hat{u}}{\partial z}, \frac{\partial \hat{v}}{\partial z}\right) = \left(\frac{S_M q}{u_\tau}\right)^2 \left(\frac{\kappa}{\ln z'/z_0}\right)^2 |\hat{\mathbf{u}}|(\hat{u}, \hat{v}),$$

as in (6b). Note that, typically, a drag coefficient $C_{z'} = (\kappa/\ln z'/z_0)^2$ is defined and $\hat{u}$ and $\hat{v}$ are reckoned at $z'$, where often $z' = 10$ m.

[B1] In the absence of waves, $D_{BF} = D_{WBR} = 0$ and it can be shown that near the bottom $P_B \cong 0$ but $P_S = u_\tau^3/\kappa z$. Also, $P_S = \varepsilon = q^3/B_1 z$, so that $q = u_\tau B_1^{1/3}$. Model constants from MY82 are $S_M = 0.39$ and $B_1 = 16.6$ so that $S_M q/u_\tau = 1$.

## REFERENCES


Apotsos, A., B. Raubenheimer, S. Elgar, R. T. Guza, and J. A. Smith, 2007: Effects of wave rollers and bottom stress on wave setup. *J. Geophys. Res.*, **112**, C02003, https://doi.org/10.1029/2006JC003549.

Battjes, J. A., and J. P. F. M. Janssen, 1978: Energy Loss and set-up due to breaking of random waves. *Proc. 16th Coastal Engineering Conf.*, Hamburg, Germany, ASCE, 569–587, https://ascelibrary.org/doi/abs/10.1061/9780872621909.034.

Blumberg, A. F., and G. L. Mellor, 1987: A description of a three-dimensional coastal ocean model. *Three-Dimensional Coastal Ocean Models*, N. S. Heaps, ed., Coastal and Estuarine Sciences Series, Vol. 4, Amer. Geophy. Union, 1–16.

Booij, N., and R. C. H. Holthuijsen, 1999: A third generation wave model for coastal regions, 1. Model description and validation. *J. Geophys. Res.*, **104**, 7649–7666, https://doi.org/10.1029/98JC02622.

Bowen, A. J., D. L. Inman, and V. P. Simmons, 1968: Wave set-down and set-up. *J. Geophys. Res.*, **73**, 2569–2577, https://doi.org/10.1029/JB073i008p02569.

Chen, T., Q. Zhang, Y. Wu, C. Ji, J. Yang, and G. Liu, 2018: Development of a wave-current model through coupling of FVCOM and SWAN. *Ocean Eng.*, **164**, 443–454, https://doi.org/10.1016/j.oceaneng.2018.06.062.

Garcez-Faria, A. F., E. B. Thornton, T. C. Lippman, and T. P. Stanton, 2000: Undertow over a barred beach. *J. Geophys. Res.*, **105**, 16 999–17 010, https://doi.org/10.1029/2000JC900084.

Govender, K., G. P. Mocke, and M. J. Alport, 2002: Video-imaged surf zone wave and roller structures and flow fields. *J. Geophys. Res.*, **114**, C07012, https://doi.org/10.1029/2000JC000755.

Grant, W. D., and O. S. Madsen, 1979: Combined wave and current interaction with a rough bottom. *J. Geophys. Res.*, **84**, 8244–8246, https://doi.org/10.1029/JC084IC04P01797.

Kumar, N., G. Voulgaris, and J. C. Warner, 2011: Implementation and modification of a three-dimensional radiation stress formulation for surf zone and rip-current applications. *Coastal Eng.*, **58**, 1097–1117, https://doi.org/10.1016/J.COASTALENG.2011.06.009.

——, ——, ——, and M. Olabarrieta, 2012: Implementation of the vortex force formalism in the coupled ocean-atmosphere-wave-sediment transport (COAWST) modeling system for inner shelf and surf zone applications. *Ocean Modell.*, **47**, 65–95, https://doi.org/10.1016/j.ocemod.2012.01.003.

Longuet-Higgins, M. S., and R. W. Stewart, 1964: Radiation stresses in water waves; a physical discussion with applications. *Deep-Sea Res. Oceanogr. Abstr.*, **11**, 529–562, https://doi.org/10.1016/0011-7471(64)90001-4.

Marsooli, R., P. M. Orton, G. Mellor, A. F. Blumberg, and N. Georgas, 2017: A coupled circulation–wave model for numerical simulation of storm tides and waves. *J. Atmos. Oceanic Technol.*, **34**, 1449–1467, https://doi.org/10.1175/JTECH-D-17-0005.1.

McWilliams, J. C., and J. M. Restrepo, 1999: The wave-driven ocean circulation. *J. Phys. Oceanogr.*, **29**, 2523–2540, https://doi.org/10.1175/1520-0485(1999)029<2523:TWDOC>2.0.CO;2.

Mellor, G. L., 2002: Oscillatory bottom boundary layers. *J. Phys. Oceanogr.*, **32**, 3075–3088, https://doi.org/10.1175/1520-0485(2002)032<3075:OBBL>2.0.CO;2.

——, 2003: The three-dimensional current and surface wave equations. *J. Phys. Oceanogr.*, **33**, 1978–1989, https://doi.org/10.1175/1520-0485(2003)033<1978:TTCASW>2.0.CO;2.

——, 2011: Wave radiation stress. *Ocean Dyn.*, **61**, 563–568, https://doi.org/10.1007/S10236-010-0359-2.

——, 2013: Waves, circulation and vertical dependence. *Ocean Dyn.*, **63**, 447–457, https://doi.org/10.1007/s10236-013-0601-9.

——, 2015: A combined derivation of the integrated and vertically resolved, coupled wave–current equations. *J. Phys. Oceanogr.*, **45**, 1453–1463, https://doi.org/10.1175/JPO-D-14-0112.1.

——, 2016: On theories dealing with the interaction of surface waves and ocean circulation. *J. Geophys. Res.*, **121**, 4474–4486, https://doi.org/10.1002/2016JC011768.

——, 2017: Reply to "Comments on 'A combined derivation of the integrated and vertically resolved, coupled wave–current equations.'" *J. Phys. Oceanogr.*, **47**, 2387–2389, https://doi.org/10.1175/JPO-D-17-0096.1.

——, and T. Yamada, 1982: Development of a turbulence closure model for geophysical fluid problems. *Rev. Geophys. Space Phys.*, **20**, 851–875, https://doi.org/10.1029/RG020i004p00851.

——, M. A. Donelan, and L.-Y. Oey, 2008: A surface wave model for coupling with numerical ocean circulation models. *J. Atmos. Oceanic Technol.*, **25**, 1785–1807, https://doi.org/10.1175/2008JTECHO573.1.

Moghimi, S., K. Klingbeil, U. Grawe, and H. Burchard, 2013: A direct comparison of a depth-dependent radiation stress formulation and a vortex force formulation within a three-dimensional coastal ocean model. *Ocean Modell.*, **70**, 132–144, https://doi.org/10.1016/j.ocemod.2012.10.002.

Newberger, P. A., and L. S. Allen, 2007: Forcing a three-dimensional, hydrostatic primitive-equation model for application in the surf zone: 2. Application to DUCK94. *J. Geophys. Res.*, **112**, C08019, https://doi.org/10.1029/2006JC003474.

O'Connor, B. A., S. Pan, J. Nicholson, N. McDonald, and D. A. Huntley, 1998: A 2D model of waves and undertow in the surf zone. *26th Int. Conf. on Coastal Eng.*, Copenhagen, Denmark, ASCE, 186–196, https://ascelibrary.org/doi/10.1061/9780784404119.020.

Phillips, O. M., 1977: *The Dynamics of the Upper Ocean*. Cambridge University Press, 336 pp.

Reniers, A. J. H. M., E. B. Thornton, T. P. Stanton, and J. A. Roelvink, 2004: Vertical flow structure during Sandy Duck observations and modelling. *Coast. Eng.*, **51**, 237–260, https://doi.org/10.1016/j.coastaleng.2004.02.001.

Roelvink, J. A., and A. J. H. M. Reniers, 1995: Lip11D Delta Flume experiments. Delft Hydraulics Rep. H2130, 106 pp.

Uchiyama, Y., J. C. McWilliams, and A. F. Shchepetkin, 2010: Wave–current interaction in an oceanic circulation model with a vortex-force formalism: Application to the surf zone. *Ocean Modell.*, **34**, 16–35, https://doi.org/10.1016/j.ocemod.2010.04.002.